3
Horse Dung and Soil-Based Composites for Construction of Aesthetic Shelves in Rural Homes of Western Rajasthan

3.1 INTRODUCTION

Reinforced composites are so traditional that they find mention in the story of the construction of Noah Ark in the Bible [Cremades, 2000]. Adobe buildings date back to 8300 B.C. [WCC, 2008]. The impregnation of mud (daub) with organic (wattle) or animal materials to improve the physical strength of mud is a very ancient technology [Ashby and Jones, 1998]. Cob is a constructional material used in England which used a mixture of sub-soil, straw and water [Saxton and Coventry, 1995]. Mixing, applying, curing and shrinkage of the cob are much dependent on the plasticity of green composite [Saxton and Coventry, 1995]. The percentage of clay or binder (less than 0.002 mm in diameter) played a major role in deciding this functionality of the cob [DMG, 1960; Greer and Short, 1995; Saxton and Coventry, 1995]. The cob and wattle-daub technique were well mastered by the English [WCC, 2008]. Soil-based materials possess the potential to provide low cost, eco-friendly and sustainable building structures [Agarwal, 1981; Benture, 1989; Coutts, 1988; Della, 1988]. The cohesive forces between soil particles impart stability to the moist earthen wall of a certain height [Mitchell and Collin, 1984]. The insertion of reinforcements within the soil will increase its bearing capacity and structural stability due to stress transfer between the grains and reinforcements [Mitchell and Collin, 1984]. Similarly, Portuguese Tabique construction used wooden structures (filled with a mixture of corn cob and mud which acted as insulators) and these timber elements were plastered with mud from outside as well as inside [Pinto *et al*., 2011].

According to UNCHS about 40% of the world lives in houses made from mud [Maini, 2010]. Recently, New Zealand revived the earth building tradition by promulgating new standards and rules. This step is the first set of standards for construction of earth buildings, Here NZS: 4297:1998 discusses the engineering design of earth building while NZS: 4298:1998 details the material and skill requirement for constructing earth buildings [WCC, 2008]. Similar to the revival of earth buildings by New Zealand, Auroville, a Non-Governmental Organization in India also described the decline in the skill set in earth construction and decline of earth construction as such towards the twentieth century [Maini, 2010]. Earth Buildings avoid pollution and are low energy users throughout their lifetime [WCC, 2008].

Figure 3.1: The MM-EO composite cantilever shelves at Arna Jharna desert museum [*Source:* Arna Jharna Desert Museum, Jodhpur, Rajasthan, India]

The use of locally available cellulosic waste by rural people may show their inherent inertia (cognitive dissonance) in adopting urban construction technology as well as materials such as cement [Lareau, 2003; Mathur, 2006; Plappally *et al*., 2011]. This inertia helps them to follow traditional practices thus preserving their culture knowledge of this construction technology [Plappally *et al*., 2011]. Some of the MM-EO structures (as illustrated in Figure 3.1) within rural indoor settings in different arid locations in Barmer, Rajasthan, India are over 20 years old. The image of the load bearing aesthetic cantilever shelf structure manufactured from this cellulose-rich composite is shown in Figure 3.1. Additives like EO are often introduced into the MM matrices to evolve novel functional characteristics and durability in the MM composites [Bentur and Mindess, 2007; Heathcote, 1995; Ren and Kagi, 1995; Weidenfeller *et al*., 2005; Bertelli *et al*., 1989]. For example, cellulosic fiber within EO when mixed with MM may cause a reduction in gross weight and handling cost respectively [Binici *et al*., 2005].

In this chapter, composites manufactured with MM-EO in a volumetric ratio of 1:1 used in the construction of light cantilever shelves is discussed. This work points towards recycling equine ordure in a meaningful way as a new bio-composite with a sustainability quotient. This chapter also concentrates on bending, densification and thermal properties. This chapter will shed light on modeling strategies of these properties for this particular cellulose-rich composites. Stochastic aspects of property development in MM-EO composite will be discussed and multi-parameter modeling strategies will be adopted for these heterogeneous particulate mixtures [Kaminskii *et al*., 1982; Soboyejo, 1965; Soboyejo, 2001]. An empirical structural analysis and microstructural study is also carried out in support of the traditional use of fifty percent by volume EO-based composites as a lightweight construction material.

3.2 EXPERIMENTAL METHODOLOGY

3.2.1 Selection of Raw Materials

The *Meth Mitti* (MM) that was used in this study was obtained from Barmer, Rajasthan India, from the small pond (locally called as *Nadi*) developed due to rainwater in monsoon. Seasonal rains provide water which may influence the said chemical weathering [Bell, 1983]. The mineralogical investigations of MM are elaborated and expounded in the subsequent section.

(a) (b)

Figure 3.2: (a) Pond soil (*Meth Mitti*, MM) local to Barmer region (b) Horse dung (EO)

MM is found as large stone like formations as shown in Figure 3.2(a). These are pulverized using a locally made wooden mallet before being soaked for a day. The other constituent is horse dung illustrated in Figure 3.2(b). As described by *Santhi* (*Sansi*) women in survey (Annexure A.1) dry horse dung is collected from the village near Arna Phanta, Jodhpur. The gathered dung is cured in the sun for almost a week to remove moisture content. Further, it is stored in the household of this nomadic community for use. The curing help to powder the dung to make uniform mixing possible and dry powdered dung is easy for handling. The stored horse dung was powdered using the wooden mallet. The horse dung is believed to be good for structural applications due to its fibrous structure compared to cow dung by *Santhi* community. The horse dung is powdered in such a way that the large organic plant material (as illustrated in Figure 3.2b) within the EO matrix remains as it is.

3.2.2 Raw Material Characterization

To identify various compounds, present and surface morphology of raw materials of bio-composites including MM and EO are analyzed using scanning electron microscopy (SEM) and energy dispersive spectroscopy (EDS) techniques of material characterization. The samples of composites at 28-days age were analyzed using x-ray fluorescence (XRF) spectroscopy. The analysis was carried out using wavelength dispersive XRF spectroscopy (Bruker S4 Pioneer) facility at AIRF, Jawaharlal Nehru University at New Delhi, India.

The groundwater used is brackish [Gopal and Bhargava, 1981; Satankar *et al*., 2017]. The water quality in western Rajasthan may even be more saline [Gopal and Bhargava, 1981]. The pH and electrical conductivity were measured using the pH meter (pH700 Eutech Instrument Ltd, India) and the electrical conductivity meter (CON 700 Eutech Instrument Ltd, India). A set of 24 samples of the source groundwater was tested for maintaining significant samples according to the central limit theorem. Flame photometer (AIM 049000, Aimil Ltd., India) was used for measuring sodium and potassium levels in the saline water samples.

3.2.3 Composite Processing

A mixture of volume fractions of MM and EO, viz. 100:0, 70:30, 60:40, 50:50 and 40:60 were used to make test samples. The measurement of volumes of raw materials were done using graduated (one liter) beakers available at the field laboratory at the Arna Jharna Desert Museum, Jodhpur, Rajasthan. The nomenclatures (as shown in Table 3.1) of these particulate composites are defined based on its constituents as M10E0, M7E3, M6E4, M5E5 and M4E6 respectively. Particulate composites made out of MM and EO are said to have isotropic properties (physical properties like fracture toughness have same measurement in different directions) according to local women folk who manufacture cantilever shelves [Ashby and Jones, 1998]. Figure 3.3 enumerates the process of manual preparation of mixture and preparation of composite. Soaked overnight MM is mixed with dry powdered EO in equal volumes uniformly and made into a green composite as shown in Figure 3.3(c). This composite is spread on a flat wooden panel as shown in Figure 3.3(d-f). Further, several similar lumps are added and a continuous finishing application is performed signifying a stochastic material design process. This would also mean a stochastic modeling approach for modeling MM-EO composite characteristics.

Table 3.1: Compositional formula for MM-EO composites

Sample	*Meth Mitti* (MM, % volume)	Equine ordure (EO, % volume)
M10E0	100	0
M7E3	70	30
M6E4	60	40
M5E5	50	50
M4E6	40	60

Thickness control and geometrical alignment is an observable feature while manufacturing. The manually pressed composite samples of length 275 mm width 105 mm and a thickness of 15 mm were cured at room temperature for 28-days. The weights of the samples were measured at an interval of 7-days each for all the distinct volume fractions defined above. Density can be easily calculated since volume of the sample is known.

The curing test of natural composites is done on the 10-15 samples of varying proportions in which the weight of the samples w, ambient temperature T_a and humidity $\emptyset_a$ measured on regular basis. The measurement records were taken for 28-days. The weight measurement was done using standard electronic weighing machine [Model Virgo, Danwer Scales, India] of accuracy 0.01 g. The ambient temperature and humidity were measured using IIT Jodhpur weather station data recorder located at the IIT Jodhpur

Ratanada, Jodhpur. These samples were also recoded for change in dimensions, density, and thermal conductivity for to understand the effect of use of EO on these physical properties. Further, thermal conductivity of the distinct specimens aged for 28-days was also studied. The guarded hot plate method (IS: 33461980) of thermal conductivity measurement was used in this case [Carlson *et al*. 2008, Eckert and Goldstein, 1976]. The interested readers are requested to refer Carlson *et al*. 2008 for detailed experimental framework.

(a) Soaked MM and dry EO (b) Mixing process (c) Mixed composite

(d) Pressing platform (e)Manual pressing (f) Sample finishing

(g) Measurement for extracting the samples (h) Sample cutting (i) Cut samples

Figure 3.3: The procedure of making the MM-EO mixure and its composite samples

3.2.4 Strength Tests of MM-EO Composites

ASTM C99/C99M standard test procedure followed to investigate the flexural strength of the specimen. For measuring the same series of three-point bending test was conducted on samples prepared from the compositions illustrated in Table 3.1. The samples were tested at an age of 7, 14, 21, and 28-days. Twenty-eight-day strength is considered following strength analysis procedures for cementitious materials as prescribed in Wilby, 2007 [Kosmatka *et al*., 2002; Wilby, 1977; IS516:2004]. To prepare the samples

specified aged specimen samples were cut and following the standard procedure and sized at 100 mm x 25 mm x 12.5 mm. While keeping on test bench the span length was kept as 80 mm on the three-point bend universal testing platform (Model EZ50 Lloyd instrument, Germany). The load application was monotonic loading which was continued till the cracks formed cause separation of samples in parts. The loading rate was maintained at 1 mm/min. The test was carried out at ambient conditions of 300 K and a relative humidity of 40%. Edge effects are neglected in this study. For the samples considered for flexural test flexural stress σ_f was calculated using Eq.(3.1) [Flin, 2007].

$$\sigma_f = \frac{3F_Q L}{2BW^2} \tag{3.1}$$

Where, F_Q is the load at the onset of failure, L is the distance between the support points (span), B is the breadth and W is width of the sample.

The compression test was carried out on the universal testing platform (Model EZ50 Lloyd Instrument, Germany) using a compression fixture. The size of the test samples was 50 mm x 25 mm x 12.5 mm. A loading rate of 3.5 N/s was applied to the failure of the sample. Test results of compression test were digitally recorded using the data acquisition enabled universal testing platform. The failure occurs when a limiting value of stress is reached and the value of compressive stress then can be calculated by Eq.(3.2) as

$$\sigma_c = \frac{F_q}{A_0} \tag{3.2}$$

Where σ_c is the compressive strength F_q is the force at the onset of failure and A_0 is the initial cross-sectional area of the sample [Flin, 2007].

The investigation on fracture toughness was measured using single-edge notched bending (SENB) in three-point bending samples. The samples were cut using a cutter and ensured by visual inspection that samples are free from defects such as pores, cracks on any damages. Then notch was created by steel saw blade on the specimens of similar size used in flexural strength test. The notch was sharpened to a 45-degree angle at the tip and root was kept flat as per standard. The process of notching was done carefully and measured using a Vernier calliper until its required size was obtained. The pre-crack length to width ratio $(a/W)$is maintained at 0.4 for these experiments, where 'a' is (depth of the pre-crack). The specimen was loaded at 3N/s on a UTM machine (Model EZ50 Lloyd Instrument, Germany). The loading span was taken to be 80 mm fracture toughness K_{I_c} was determined from the expression of Eq.(3.3) of ASTM E-399 standard [Soboyejo, 2003; Azeko *et al*., 2015].

$$K_{I_c} = f\left(\frac{a}{W}\right) Y_f \sqrt{\pi a} \tag{3.3}$$

Where,

$$\left(\frac{a}{W}\right) = \frac{3\left(\frac{a}{W}\right)^{0.5}\left[1.99 - \left(\frac{a}{W}\right)\left(1 - \frac{a}{W}\right)\left(2.15 - 3.93\frac{a}{W} + 2.7\frac{a^2}{W^2}\right)^{1.5}\right]}{2\left(1 + 2\frac{a}{W}\right)\left(1 - \frac{a}{W}\right)^{1.5}} \tag{3.4}$$

Further, to find surface roughness of the composite samples considered in this experiment hybrid measuring instrument for surface roughness and contour measurement (Mitutoyo, USA) was used. The samples similar to prepared for strength tests discussed above. In this technique the sample surface was were exposed to the probe of device which record the surface roughness and provide results.

3.3 RESULTS AND DISCUSSIONS

3.3.1 Water Characterization

Ca2+ and Mg2+ concentrations were found using ethylene-di-amine-tetra-acetic acid (EDTA) titration tests. Table 3.2 illustrates the characteristics of groundwater used in this study and values of parameters found in Jodhpur district (Arna Jharna desert museum, Karwar and Badarli village) ground water samples [Jain, 2014]. Saline water available across western Rajasthan had been used traditionally for

ages in pottery and rural construction. Soaked MM is mixed with equal volume of EO for traditional shelf manufacture illustrated in Figure 3.3.

The description of salinity of groundwater is beyond the purview of this chapter. Hence the readers are encouraged to read about the brackishness of groundwater in Rajasthan from Gopal and Bhargava, 1981. The availability of brackish water across the state can be correlated with the design and local development of this MM-EO composite mix technology for construction.

Table 3.2: Measurement of groundwater quality characteristics used for the manufacture of MM-EO composite samples [Jain, 2014]

Parameter	Minimum value	Maximum value	Observed value (in present study)
pH	7.29	8.7	7.65
EC (µS/cm)	470	17770	17930
TDS (mg/l)	260	11505	9600
CaCO3 (mg/l)	150	1360	-
CO3 (mg/l)	0	192	-
HCO3 (mg/l)	28	2202	-
Cl (mg/l)	28	4880	5583
SO4 (mg/l)	16	994	2214
NO3 (mg/l)	8.58	650	31
Ca (mg/l)	21	283	190
Mg (mg/l)	10	193	21
Na (mg/l)	19	3900	1731
K (mg/l)	0.1	98	560
F (mg/l)	0.2	4	2.56
Fe (mg/l)	0	3.5	0.08
SiO2 (mg/l)	10	48	36
PO4 (mg/l)	0	6.42	0.08

3.3.2 Characterizing MM, EO and MM-EO Composite

The matrix part of the composite is made using MM. The surface morphology and EDS spectrum of the MM depict resemblance to the phyllo-silicates group [Welton, 2003; Satankar *et al*., 2018]. Figure 3.4(a) illustrates distinct and separate flakes kept one over the other indicating a sheet or layered structure. Table 3.3 presents the elemental detection in MM and as shown in the spectra of Figure 3.4(b) it supports the possibility of the presence of silicate sheets bonded with cations (Ca and Fe) [Nelson, 2015].

The presence of calcium carbonates crystals adhering to the cellulosic fibers is illustrated in micrograph in Figure 3.5(a). The EDS spectra in Figure 3.5(b) and Table 3.4 together confirm the presence of calcium in EO. Calcium carbonate along with the cellulose content makes EO a good reinforcing agent, thus producing strong fibrous network between the matrix and the reinforcement material [Cho *et al*., 2016]. This would mean an increase in $CaCO_3$ would prevent failures due to bending fractures [K-tron, 2014]. The composites with cellulose interacting with calcium carbonate exhibit adsorption of calcium carbonate onto cellulosic fibers in aqueous media [Dalas *et al*., 2000; Fimbel and Siffert, 1986]. The adsorption kinetics is beyond the scope of present work. Thus, this composite finds potential application in paper manufacturing industry [Cheng *et al*., 2016]. This also would mean that animal dung such as equine ordure is an optimal material for use in paper manufacturing [Cox, 1952; Njeru, 2016].

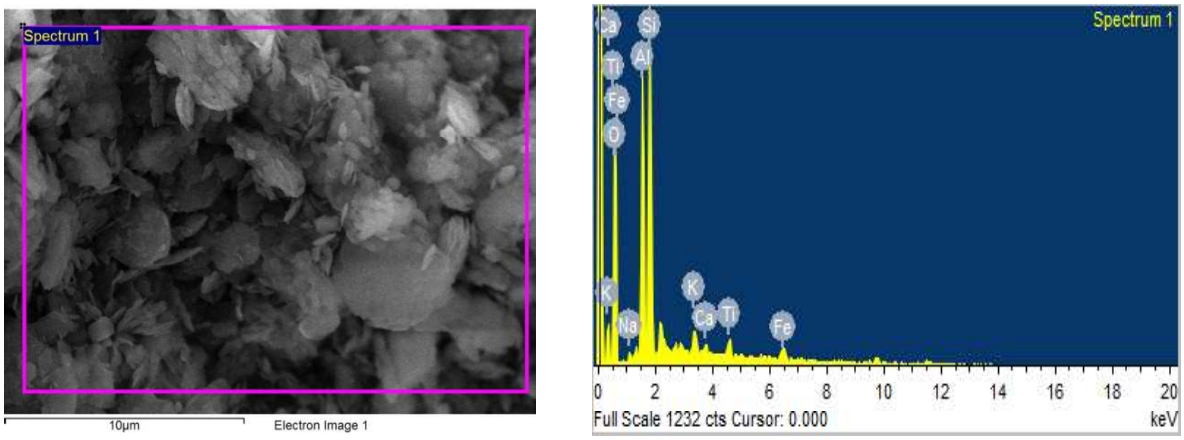

(a) (b)

Figure 3.4: (a) SEM micrograph of MM (b) EDS spectra of MM [Carl Zeiss EVO 18 SEM, IIT Jodhpur]

Table 3.3: Chemical composition (weight % and atomic %) of MM (EDS, Carl Zeiss EVO 18 SEM, IIT Jodhpur)

Element	Weight %	Atomic %
O	53.81	68.37
Na	0.79	0.70
Al	14.86	11.19
Si	22.43	16.23
K	1.90	0.99
Ca	0.82	0.42
Ti	2.19	0.93
Fe	3.20	1.17
Total	100.00	

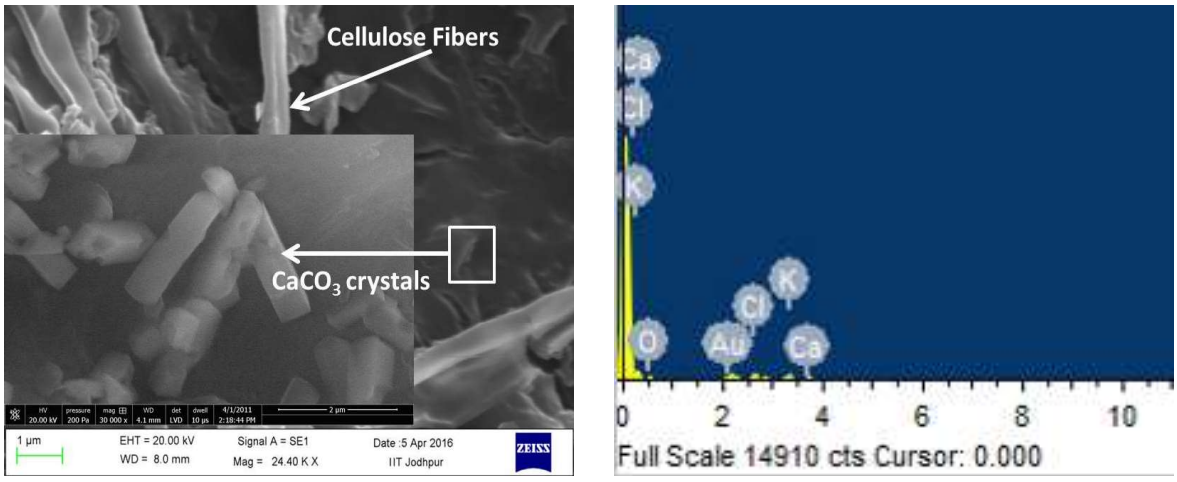

(a) (b)

Figure 3.5: (a) FESEM micrograph of EO [Carl Zeiss EVO 18 SEM, IIT Jodhpur] (b) EDS spectra of EO [Carl Zeiss EVO 18 SEM, IIT Jodhpur]

Table 3.4: Chemical composition (weight % and atomic %) of EO (EDS, Carl Zeiss EVO 18 SEM, IIT Jodhpur)

Element	Weight %	Atomic %
O	50.37	69.79
Mg	0.70	0.64
Al	1.56	1.28
Si	9.65	7.61
Ca	36.53	20.21
Fe	1.20	0.47
Total	100.00	

Table 3.5 shows comparatively higher molecular SiO_2 present in M5E5 which may provide an edge to improving its physical properties and strength properties compared to other composites. M5E5 contains the maximum SiO_2 content making it least bio-active compared to other distinct samples. The MM-EO composites can be considered as bioactive material because of the high ratio of CaO to P_2O_5 content and low (less than 60%) SiO_2 [Marikani *et al.,* 2008]. Manual manufacture of the such composite is feasible since presence of alkaline elements in groundwater used in the preparation of the blend leads to permeation of sodium oxides into the composites [Gopal and Bhargava, 1981; Satankar *et al.,* 2017; Wang, 2003]. Composites therefore show (because of High K_2O/Na_2O ratio) clayey (moldable and impervious to water) character [Marikani *et al.,* 2008]. Highly reactive oxides of Ca, K and Na oxide show a fractional decrease in volume with increase in EO in the samples as observed from Table 3.5.

Table 3.5: Chemical composition (in weigth %) of distinct MM-EO composites at 28-day age (XRF, Bruker S4 Pioneer facility at AIRF, Jawaharlal Nehru University at New Delhi, India)

Element(s)	M10E0	M7E3	M6E4	M5E5	M4E6
SiO_2	52.87	52.27	50.48	56.87	56.67
Al_2O_3	22.14	19.62	18.6	21.44	21.89
$Fe2O_3$	1.15	1.63	1.5	1.57	1.47
CaO	1.82	1.74	1.49	1.32	1.18
K_2O	1.45	1.62	1.26	1.25	1.15
TiO_2	1.59	1.47	1.35	1.53	1.61
MgO	0.84	0.82	0.76	0.84	0.77
Na_2O	0.57	0.61	0.47	0.59	0.47
P_2O_5	0.18	0.2	0.16	0.15	0.14
MnO	0.02	0.02	0.02	0.02	0.01

3.3.3 Density and Thermal Conductivity of MM-EO Composites

It is very significant to note that in Figure 3.6 thermal conductivity of pure MM is almost mirrored again after an addition of 50% volume fraction of equine ordure. This also means that preservation of the thermal property of a specific volume of MM is performed by addition of the same volume of EO. This attests the fact that selection of specific volume fraction MM and EO for manufacturing the composite can help design controlled thermal environments [Xu *et al.,* 2003]. It can also be noted that thermal conductivity dips with an increase in equine ordure from zero to forty percent and then again regains with further increase in the volume of EO to sixty percent.

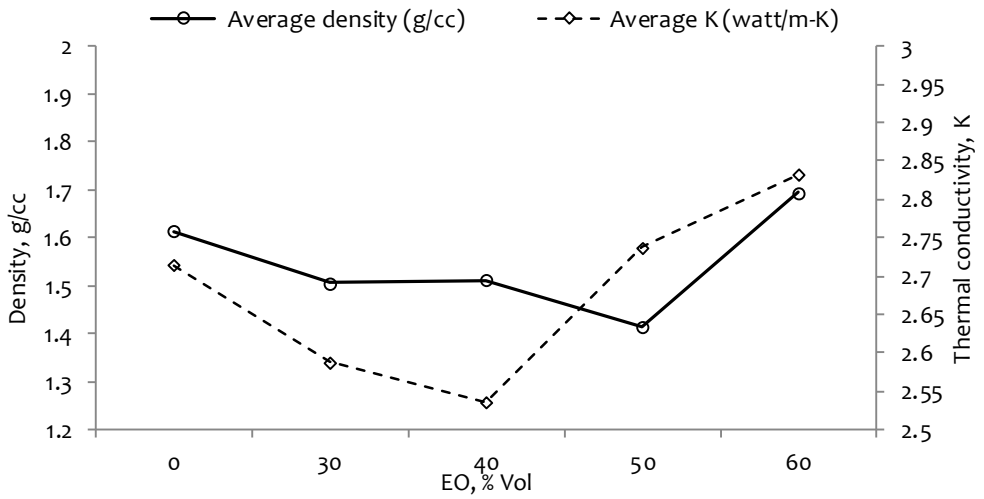

Figure 3.6: Variation of density and thermal conductivity in the MM-EO composites

(a) Thermal Conductivity Modeling

From the framework of quotient response modeling developed in Plappally *et al.*, 2011, for better prediction of thermal conductivity, mass is assumed to be an observable variable in the development of thermal conductivity probabilistic model. Therefore, a new variable G_K is defined and can be written as Eq. (3.5) [Sussman, 1976; Plappally *et al.*, 2009; Plappally *et al.*, 2011].

$$G_K = \frac{X_i}{Y_K} \tag{3.5}$$

Here X_i is the mass of the EO-MM composite whose thermal conductivity Y_K is to be calculated. Then G_K can be predicted and written in the form of Eq.(3.6) .

$$G_K = 0.519 + 0.00115 lnX \tag{3.6}$$

The above new variable is predicted using regression Eq.(3.6) has a coefficient of determination R^2 of 80.9% and a model error s of 0.00088 (Minitab 16, IIT Jodhpur License). The distribution defined for G_K is acceptable since the Anderson-Darling test statistic is 0.282 is less than the c_α critical of 1.321 for exponential distribution of G_K at a level of significance of 0.05 [Ang and Tang, 2006]. Interested authors are requested to refer Table A6(b) for exponential distribution related tables of Anderson-Darling test statistic in Ang and Tang, 2006. In Figure 3.6 density is plotted along with thermal conductivity since mass is an observable quantity in these composites. It is to be understood that densification of such materials is a stochastic process [Kaminskii *et al.*, 1982].

(b) Density modeling

It is important to note from Figure 3.6 that density for MM-EO composites decreases with a steep slope within a week and then follows an asymptote [Kou and Kou, 2003; Plappally *et al.*, 2009]. This transient fall in density D_i can be easily related to its prior development D_{i-1} as a function of T_i for $i = 1,2,3 \ldots n$ [Kaminskii *et al.*, 1982]. This can be expressed by Eq.(3.7) as,

$$\frac{D_i}{D_{i-1}} = {T_i}^{{\kappa_i}^4} \tag{3.7}$$

Here, κ_i is a transfer model constant and $T_i^{\kappa_i}$ becomes a transfer function [Plappally, 2010]. Due to the heterogeneity of constituents of the MM-EO composite, then density decreases independently from time to time. Thus, the curves in Figure 3.6 represent discrete time birth-death process [Soboyejo, 1965].

If density D_i is transformed using T_i in the following manner then quotient characterizes both density D_i and T_i respectively [Sussman, 1976; Plappally *et al.*, 2011]. The transformation equation can be expresses using Eq.(3.8) as,

$$Y_d = \frac{T_i}{D_i} \tag{3.8}$$

Table 3.6: Modelling density variation as a function of time

MM-EO Samples/ Coefficients	ε_i	ϕ_i	R^2	Error, s
M7E3	-0.0488	0.764	99.9	0.249
M6E4	-0.306	0.813	99.9	0.244
M5E5	-0.408	0.878	99.3	0.729
M4E6	-0.392	0.881	99.2	0.792

The new variable Y_d will characterize non-linearity of the density of MM-EO composites. This would mean that linearization is required to define this new variable [Cox and Miller, 1965; Soboyejo, 1965]. This linearization is written in the form of Eq.(3.9) as,

$$Y_d = \varepsilon_i + \phi_i T_i \tag{3.9}$$

Here, ε_i and ϕ_i are coefficients representative of a MM-EO composite with a distinct composition and time respectively. The linearization this developed for the different MM-EO composite developed are tabulated in Table 3.6. It is important to characterize the stochastic evolution of density of all different MM-EO composites using a generalized equation. In order to perform the framework developed by Soboyejo *et al*., 2001 is utilized. Here, the coefficient representative of an MM-EO composite with a distinct composition C_i is considered as a new parameter and the Eq.(3.9) is rewritten in the form of Eq.(3.10) [Haldar and Mahadevan, 2000; Plappally *et al*., 2010].

$$Y_d = a_i + d_i T_i + e_i C_i \tag{3.10}$$

Here a_i, d_i, and e_i represent the coefficient of model, time, and the newly derived parameter characterizing distinct MM-EO composites. Table 3.7 illustrates the coefficient of determination of the model elaborated using Eq.(3.10).

Table 3.7: Modelling density variation in MM-EO composites as a function of independent variables time and parameter characterizing these composites

Variables/ Coefficients	a_i	d_i	e_i	R^2	Error, s
T_i	-0.289	0.834	-	98.7	0.91
C_i	-1.31	0.834	-3.51	99.1	0.75

The model presented in Eq.(3.10) and related numerical elaboration in Table 3.7 is verified using a variance analysis test from Eq.(3.11) as,

$$Var\ Y_d = d_i^2 Var\ T_i + e_i^2 Var\ C_i \tag{3.11}$$

$$Var\ Y_d = 65.74 \approx (0.834)^2 \times 93.33 + (-3.51)^2 \times 0.021 \tag{3.12}$$

It is important to note that the variability in density due to time $d_i^2 Var\ T_i$ is large compared to that of the individual MM-EO composition effects, $e_i^2 Var\ C_i$ which can be verified from Eq.(3.12) [Plappally *et al*., 2009; Plappally *et al*., 2011; Soboyejo, 1968].

3.3.4 Weight Variation in Composites

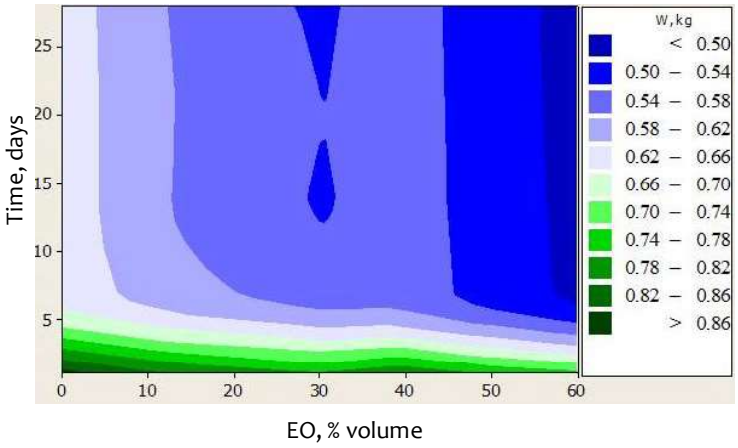

Figure 3.7: The variation of the weight of MM-EO samples with age and composition (Minitab 16 software, IIT Jodhpur License)

As described earlier, weight reduction of 10-15 samples of each composition was recorded until the change in weight was found approximately negligible (28-days in this case). Weight reduction of all the samples is illustrated in Figure 3.7. This elaborates a negligible change in weight of samples with approximately 45-55% by volume of EO. The variation of weights is in the range 0.50-0.54 kg for 50:50 composition from almost the fifth day of curing. This invariable weight of the M5E5 composite supports its use for construction by rural people. It is important to understand that volume fraction of the constituent, the micro-climate (humidity and temperature variation in the specific geographic location of composite manufacture or immediate environment) and time play an important role in defining the weight of the sample [Bentur and Mindess, 2007; Satankar *et al*., 2017]. The above discussion strengthens the concept of density variation in MM-EO composites due to shrinkage or volume change [Wilby, 1977].

A large decline in sample weights was reported to be occurring between the first week and second week of curing. This weight reduction attributed to the loss of moisture from the composites. After the second week the weight loss phenomenon diminishes and goes asymptotic. This phenomenon refers to the maximum loss of water that could occur at a certain range of temperature and humidity. The maximum variation in weight observed for the sample containing an equal volume of its constituents. Figure 3.8 enumerates variation of humidity and temperature over 28-days.

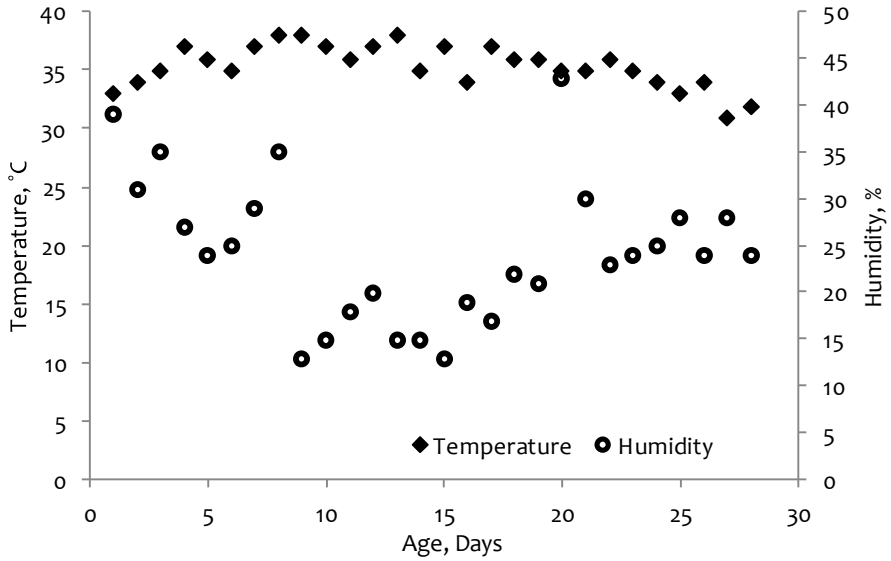

Figure 3.8: The variation of humidity and temperature during the 28-days period of MM-EO composite curing experiments conducted at Jodhpur

From Figure 3.7 and Figure 3.8 it can be inferred that MM-EO composite weight at any time is a nonlinear function of temperature and humidity of the location. These values of humidity and temperature influence water loss and hence the weight of the sample. Therefore, a multiplicative modeling approach may be adapted to predict the weight of composites at any given time [Wilby, 1977]. It is expected to predict weight w_c of samples during aging. Here age X_1, temperature X_2, and humidity X_3, are the variables that may influence the weight Y_c. Then the multiplicative model can be generally expressed by Eq.(3.13) as,

$$\ln Y_c = \beta X_1^{\beta_1} X_2^{\beta_2} X_3^{\beta_3} \tag{3.13}$$

Table 3.8: Multi-parameter regression framework with a coefficient of determination and error of the model represented by Eq.(3.13)

Samples	β	β_1	β_2	β_3	R^2	Error, s
M7E3	7.227	-1.10749	0.0165	0.00081	99.86	0.036
M6E4	7.156	-1.10749	0.0187	0.00076	99.86	0.0388
M5E5	7.169	-1.10749	0.0187	0.00084	99.86	0.367
M4E6	7.123	-1.10992	0.0162	0.00088	99.85	0.0388

The framework followed in the development of the model is discussed in chapter-2 [Dubey *et al*., 1997]. By utilizing the data in Figure 3.8 the Eq.(3.13) can be rewritten in the form of Eq.(3.14).

$$Y_c = \frac{e^{\beta+\beta_2 X_2+\beta_3 X_3}}{X_1^{\beta_1-1}} \tag{3.14}$$

Here Y_c is the response variable and is defined as $Y_c = \frac{w_c}{T}$ while β_1, β_2 and β_3 represent coefficients for the corresponding predictor variables defined above. All the coefficients values, the coefficient of determination R^2 and model error s in the model values are represented in Table 3.8. For a general formulation to the model curing process, the material effect of MM and EO needs to be incorporated. The material properties are inherited within the model constant β is enumerated in Table 3.8. Therefore, this model constant also becomes a new parameter in the general formulation. This mathematical modeling framework was proposed by Soboyejo *et al*., 2001. The mathematical framework is elaborated and the interested researchers are requested to refer Soboyejo *et al*., 2001. Then model to predict the weight of samples while aging can again be re-written by Eq.(3.15),

$$Y_c = \frac{e^{\mu_0+\nu_1 X_2+\nu_2 X_3+\nu_3 X_4}}{X_1^{\gamma_1-1}} \tag{3.15}$$

Table 3.9: Regression framework with a coefficient of determination and model error for Eq.(3.15)

Parameter	μ_0	γ_1	ν_1	ν_2	ν_3	R^2	Error, s
V_1	6.565	-1.1013				99.22	0.081
V_2	6.2485	- 1.1013	0.00575			99.72	0.049
V_3	6.9342	- 1.1067	0.00575	- 0.0190		99.85	0.036
V_4	9.92	- 1.1067	0.00702	- 0.0190	- 0.426	99.86	0.035

In Eq.(3.15) X_1 represents age, X_2 represents EO composition, X_3 represents temperature, and X_4 represents variable derived model constant β from Table 3.8. These variables are found to be correlated to each other [Bhalerao *et al*., 2003]. The multivariate analysis helps in deriving independent predictor

variables [Plappally *et al*., 2011]. In Eq.(3.15), Y_c denotes the response variable $\frac{w_c}{T}$ and independent variables V_1 represent age, V_2 represents volume fraction of MM, V_3 represents temperature, and V_4 represents independent variable derived model constant α_0 from Table 3.8 following the transformed equation.

Further, in Eq.(3.15), v_1, v_2, v_3 and γ_1 represent coefficients for the independent predictor variables respectively, while μ_0 is model constant. From Table 3.9, age emerges as most significant process parameter for the weight reduction. The proposed model provided in Eq.(3.15) used in prediction of weight in curing has R^2, 99.86% and s, 0.0355 which seems acceptable. Figure 3.9 shows a comparison of weight loss during curing process for experimental and prediction using Eq.(3.15) for each week.

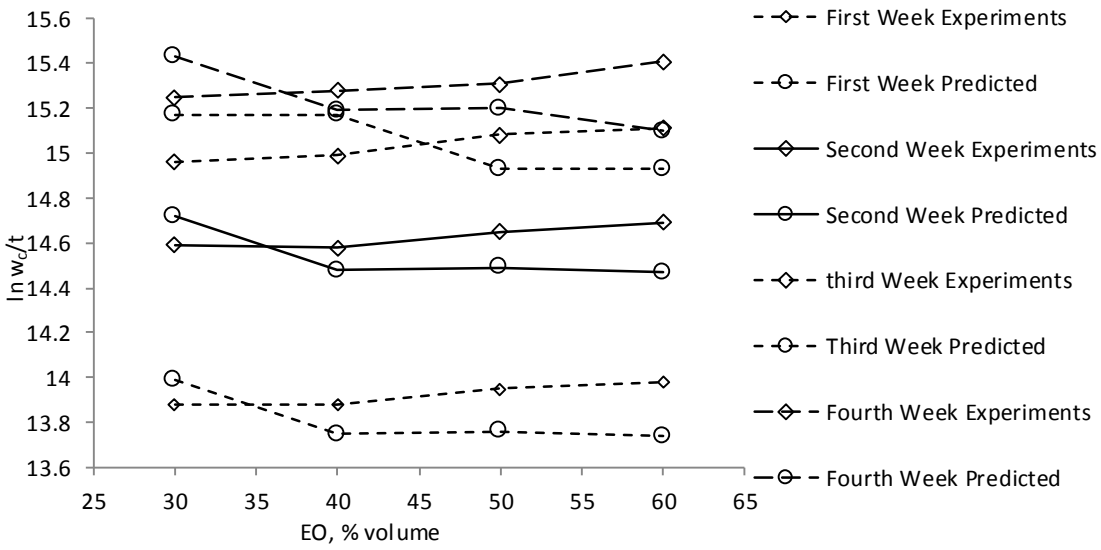

Figure 3.9: Comparative analysis of weight loss during curing experiments and prediction using Eq.(3.15)

3.3.5 Modeling Flexural Character

It is known that incorporation of cellulosic fibers within the load-bearing composites increases their tensile response [Markovich *et al*., 2001]. From Figure 3.11 MM-EO composites samples are found to gain flexural strength after two weeks of curing at room temperature. It is found that the M5E5 attains better flexural strength than concrete when taken as a function of a very low maximum service temperature [Ashby, 2006]. Further, the flexural strength was on par with those of rigid polymer foams at the end of 28-days [Ashby, 2006].

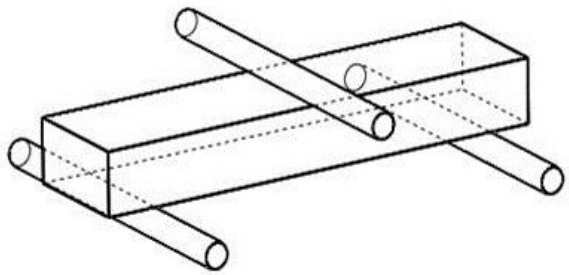

Figure 3.10: Representation of three-point loading framework for rectangular specimens

Figure 3.10 provides the loading style during a three-point bend test for flexure or fracture toughness. The overall increase in strength (as shown in Figure 3.11) is be due to frictional interaction between the reinforcing elements and the composite matrix [Bower *et al*., 2016]. In the present case, the inclusion of EO into MM composite matrix may also affect the shrinkage behavior in composites [Bower *et al*., 2016]. This is in contention of the fact that calcium carbonate content will help improve shrinkage properties and with time [Arencón and Velasco, 2009]. Interaction time of calcium carbonate and cellulose

after the process of molding (as shown in Figure 3.11) influences flexural behavior and strength [Arencón and Velasco, 2009].

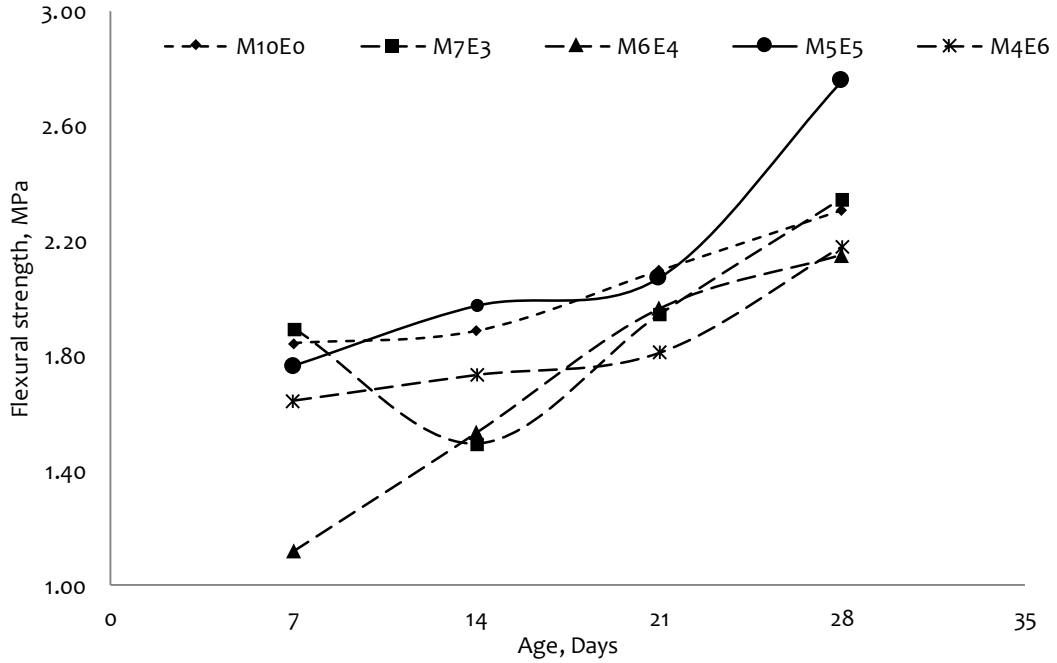

Figure 3.11: Development of flexural strength in MM-EO composites with time

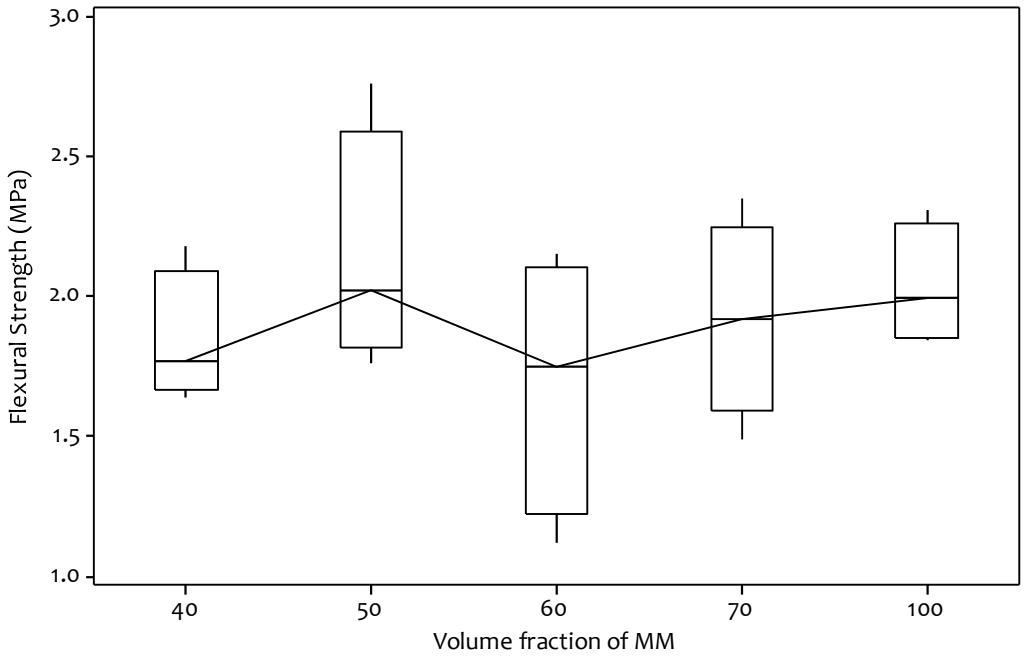

Figure 3.12: Flexural strength box plot of MM-EO composite for 28-day period corresponding to the Figure 3.11

In randomly reinforced fiber composites, the strength and thermal properties are said to be dependent on its constituents and their volume fractions respectively [Chamis, 1972]. Here, it is important to understand the most observable variable for development of flexural strength is time and hence following the new variable Q_f can be defined by Eq.(3.16) as,

$$Q_f = \frac{T_i}{\sigma_f} \tag{3.16}$$

Here, σ_f is the measure value of flexural strength enumerated in the Figure 3.12 and T_i is the age of curing and consequent testing of the MM-EO composite samples. Then, Q_f can be predicted by Eq.(3.17) [Haldar and Mahadevan, 2000],

$$Q_f = -6.39 + 5.55.\, lnT_i \tag{3.17}$$

The coefficient of determination of the prediction Q_f using Eq. (3.17) is 91.4% with a model error of 0.932. The distribution defined for Q_f is acceptable since the Anderson-Darling test statistics is 0.559 is less than the c_α of 1.321 for the exponential distribution of the flexural strength data (as shown in Figure 3.11) at a confidence of α-0.05 [Ang and Tang, 2006]. Interested authors are requested to refer Table A6(b) for exponential distribution related tables of Anderson-Darling test statistic in Ang and Tang, 2006.

3.3.6 Modeling Compressive Strength

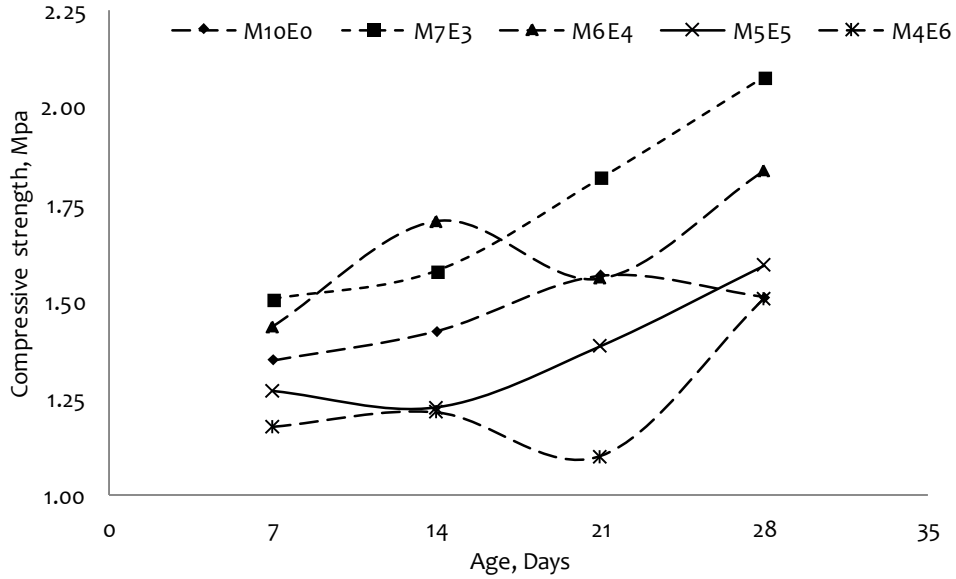

Figure 3.13: The compressive strength of MM-EO composite as a function of initial volume fraction of water used to manufacture distinct composites

Figure 3.13 illustrates that samples prepared with 35% and 25% water (by volume of MM content) respectively, improved in their compression attributes after second week of curing. Further, from Figure 3.14 it is observed that the compressive strength properties of composite without EO mirror with the compressive strength values of M5E5. This similarity will also be one of the reasons for use of such a composition which can retain the properties of 100% MM based composites after a 28-day period. This would mean that this composition may sustain similar compressive character σ_c with time.

The samples manufactured with 30% and 20% water by volume of MM showed alternating increase during even number of weeks and decrease in compressive strength during weeks of curing respectively. The compressive strength is found to be a non-linear function of age [Morel *et al.*, 2001]. It is found that most of the samples tested here achieve at least 75% of the M7E3 strength due to similarity in the direction of material transport during their manufacture [Plappally *et al.*, 2011]. With the framework developed by Plappally *et al.*, 2011 a model for predicting the compressive strength σ_c can be expressed in terms of a new variable Y_{com} by Eq.(3.18),

$$Y_{com} = \frac{T}{\sigma_c} = \in T^{\delta_1} X_{mm}^{\delta_2} \tag{3.18}$$

Table 3.10: Regression model for prediction of flexural strength of MM-EO composites as a function of T and X_{mm}

Parameter	∈	δ_1	δ_1	R^2	Error, s
T	0.047	0.822	0	88	0.172
X_{mm}	2.72	0.835	-0.663	91.7	0.145

Table 3.10 illustrate the coefficient of determination of the model elaborated using Eq.(3.18). Here T is the ambient curing age of the MM-EO composite in days, ∈ is the model constant, δ_1 and δ_2 are the coefficients of variables curing age T and volume fraction of MM X_{mm} respectively. Eq.(3.18) can also be represented in a tabular format. Even though the variable X_{mm} and T are insignifcantly correlated, it is important that correlation free variables (new independent variables derived using multivariate analysis) are used for prediction by Eq.(3.19) [Plappally *et al*., 2011; Plappally, 2010].

$$Y_{com} = T_1/\sigma_c = \in_1 T_1{}^{g_1} X_{1mm}^{g_2} \tag{3.19}$$

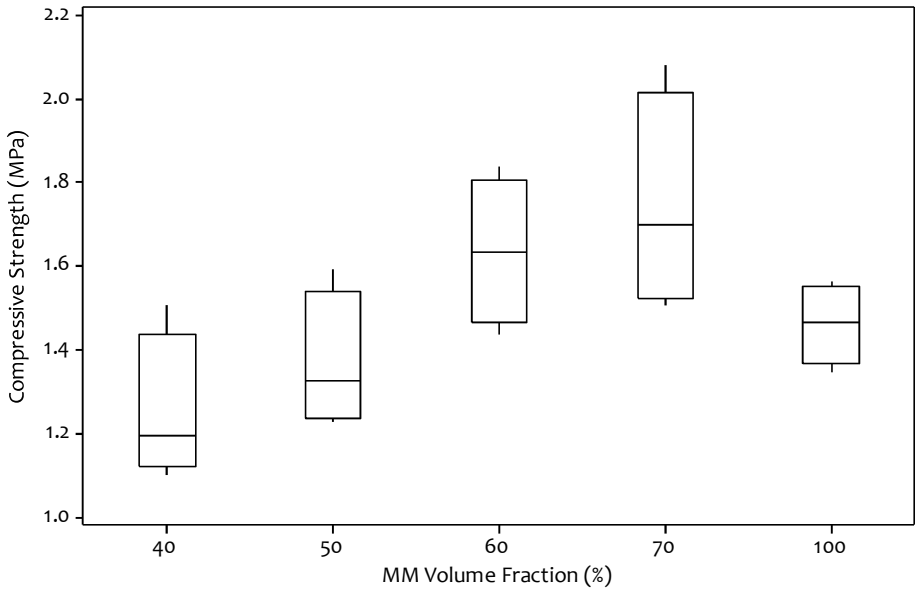

Figure 3.14: Compressive strength box plot of MM-EO composite for 28-day period corresponding to the Figure 3.13

Here, $\in_1$ is having the value 2.2 the coefficients of correlation free variable T_1 and X_{1mm} are g_1 and g_2 with numerical values 0.266 and 0.4 respectively. This would mean that both age and volume fraction of MM had a positive influence on compressive strength development. Further, the dominant influencing parameter for compressive strength development is of the volume fraction of MM in the composite. The maximum discrepancy D_{max} is 0.145 between cumulative frequency of experimental values of Y_{Com} to the cumulative frequency of multiplicative distribution in equation above is less than critical value of theoretical D_n^{α}≈0.155 for n=47 and significance level α=0.02 recommended by Kolmogorov-Smirnov [Ang and Tang, 2007]. This means that Eq.(3.19) is acceptable for modeling compressive strength of only MM-EO composite materials.

3.3.7 Fracture Toughness of MM-EO Composite

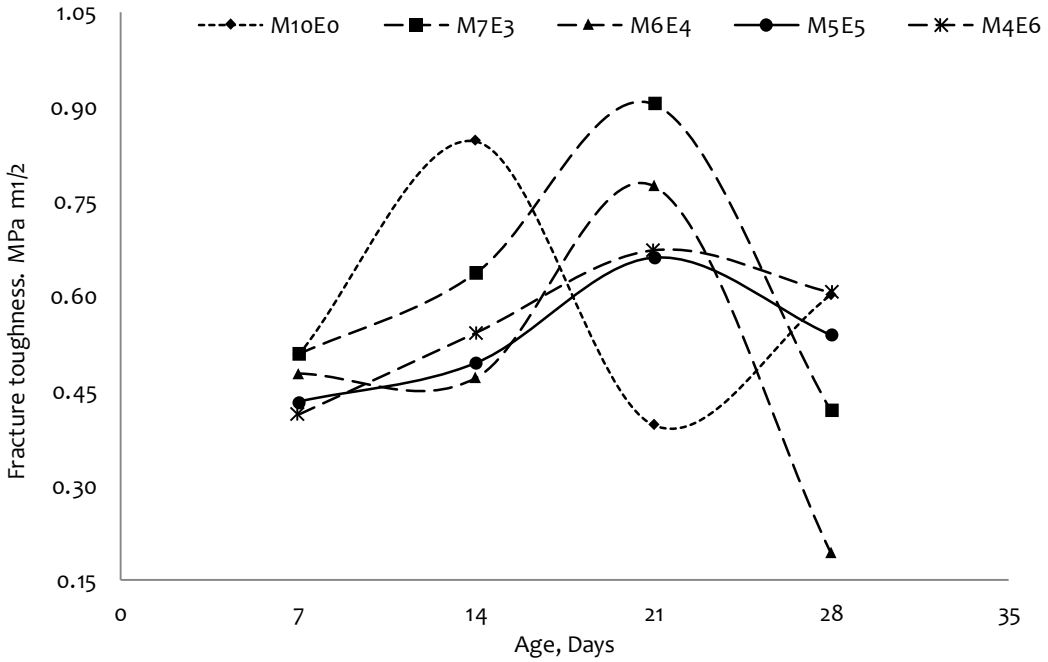

Figure 3.15: Bi-modal distribution of fracture toughness with age

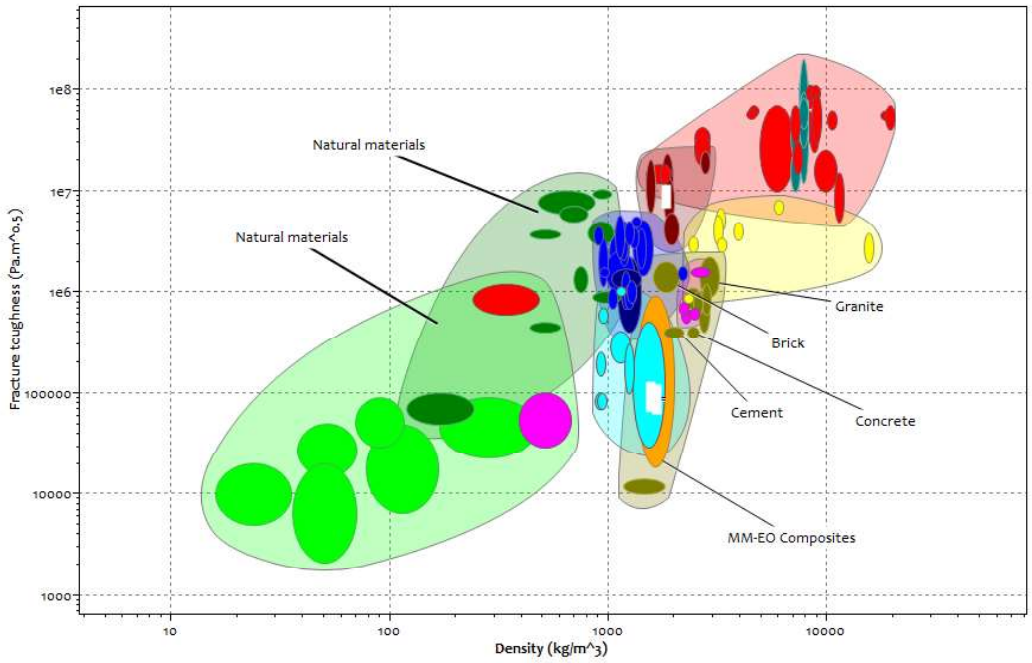

Figure 3.16: Plot of fracture toughness as a function of density for MM-EO composite

It is to be noted that smaller the particles better the fracture toughness in particulate composites [Lauke, 2009]. Figure 3.15 illustrates the bi-modal fracture toughness distribution for similar volume fraction MM-EO samples [Nevasmaa *et al*., 2005]. A distinct yet increasing trend in fracture toughness is observed for the first three weeks and then a sudden decline is noted for the families of M5E5-M4E6 and M7E3-M6E4 respectively. Similar variation in fracture toughness was observed by Dongming *et al*., 1994 in particulate polypropylene and $CaCO_3$ composite. Wong *et al*., 2009 enumerates a similar visual illustration of fracture toughness for wood flakes reinforced polyester and sand particle reinforced polyesters. Here the CES Edupack software package is used to plot the fracture toughness of MM-EO equal volume fraction

composites alongside of all other different materials studied by Ashby, 2006 such as concrete, cement, bricks etc. in the Figure 3.16.

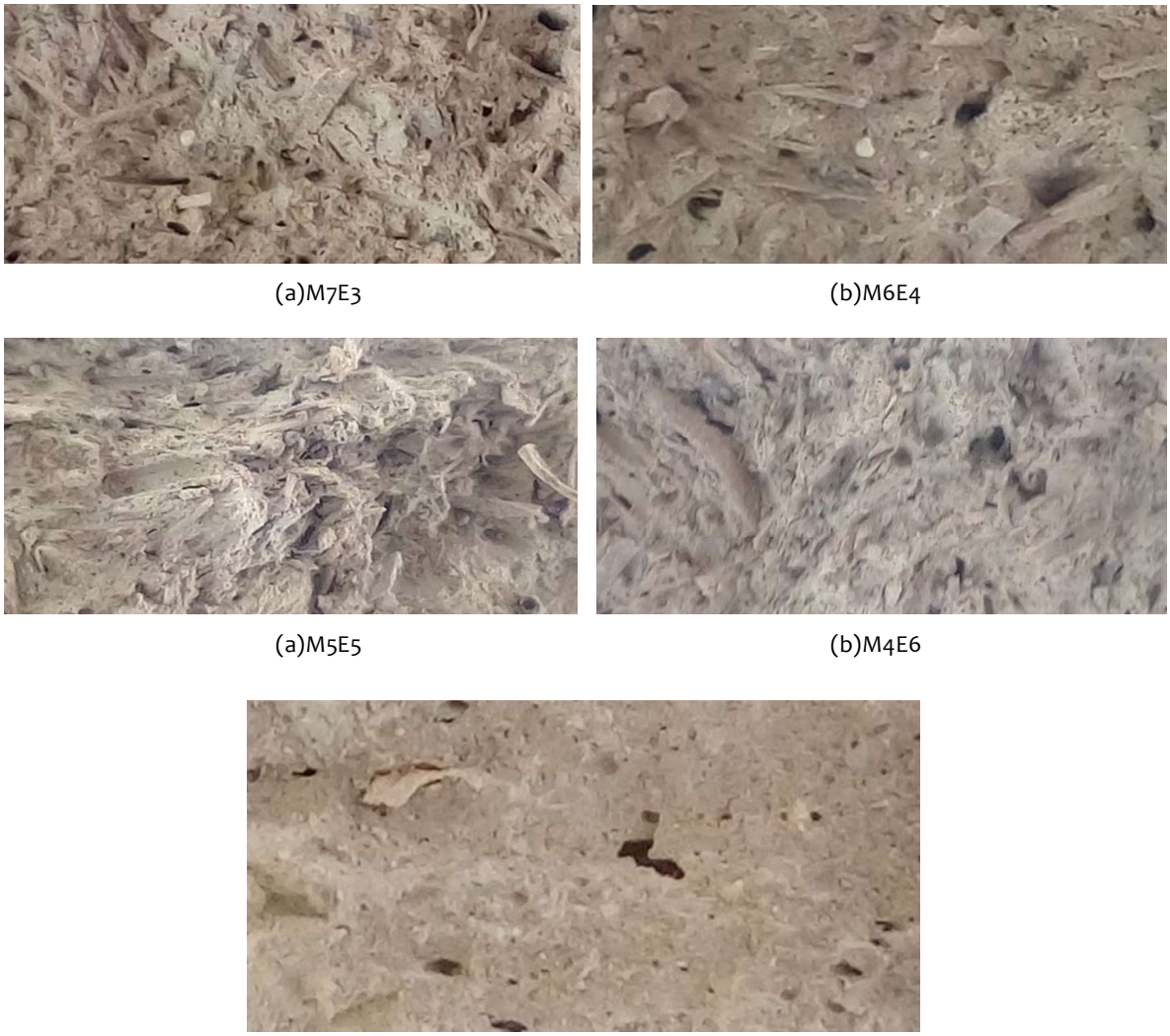

(a)M7E3 (b)M6E4

(a)M5E5 (b)M4E6

(a)M10E0

Figure 3.17: Fractured surfaces of MM-EO composites (M10E0, M7E3, M6E4, M5E5 and M4E6) observed using a 4X optical zoom camera

The basic toughening mechanisms observed in these particulate composites are increase of roughness of the surface and crack being trapped by the fibers [Qiao, 2003]. From Figure 3.17 it can be observed, for example, that the fractured surface M7E3 sample contains numerous small non-uniform and random pits from which the cellulosic fibers might have sheared or slide away during the single edge notch bend test [Zum Gahr, 1998]. It is very difficult to predict fracture toughness with the fractured profiles of the samples shown in Figure 3.17. Therefore, with the notion and belief of the community that the surfaces can provide an effective prediction of the strength of the MM-EO composites, rather than looking at the fractured surfaces the formed surfaces are taken into consideration [Rider, 1998].

Therefore, the surface roughness study of a non-fractured surface of 28-days cured samples is considered as the prominent way to define fracture toughness character of these composites and plotted in Figure 3.18. for distinct volume fractions of MM. The positive error bars in Figure 3.19 from the range of the M5E5 samples roughness show the maximum roughness gained by M4E6. Similarly, the negative error bars represent the roughness of the M7E3 composites.

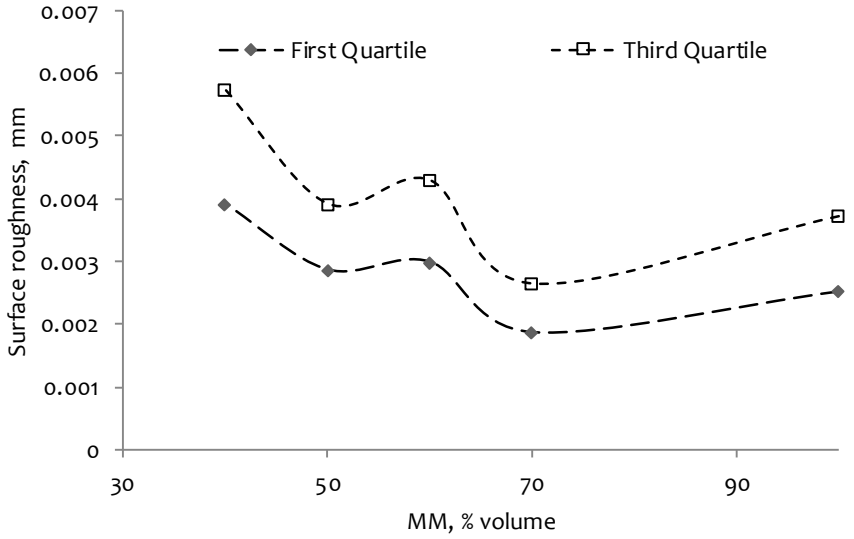

Figure 3.18: The first and third quartile values of surface roughness of the distinct samples of MM-EO composite

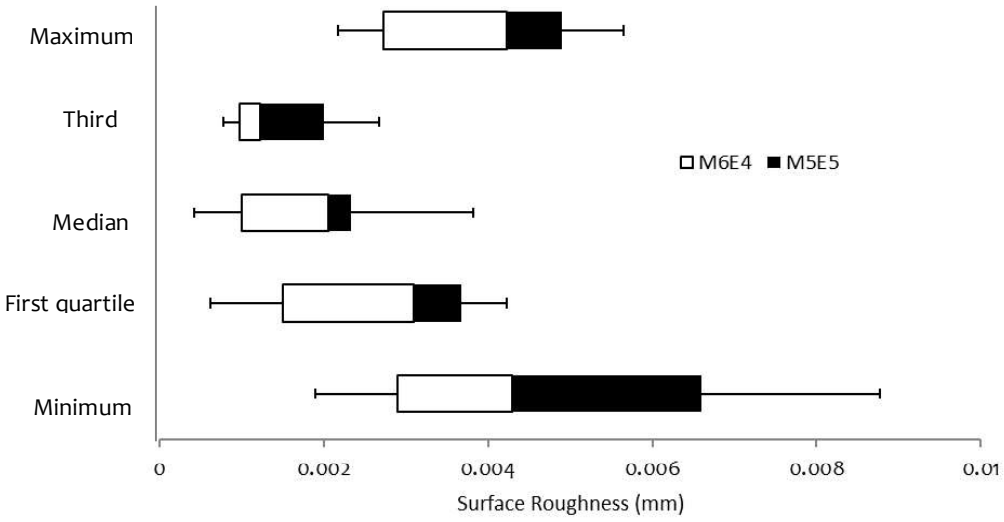

Figure 3.19: The roughness values of M5E5 specimen surfaces compared with surface roughness of other specimens

In the M6E4 sample of the MM-EO composite, an increase in the size of pits is observed or in other words, creation of small number of large valleys due to cellulosic fiber pull-out is observed. Figure 3.20 illustrates the extended cellulosic fiber protruding from the cracked surface of the M5E5 specimen which create numerous small pits on the specimen's crack surface due to fiber pull out [Mustapha *et al.,* 2015; Sockalingam and Nilakantan, 2012; Zhandarov and Mader, 2005; Zhandarov *et al.,* 2001].

When the fracture surface of composite samples with equal volume of MM and EO are observed, uniform spread of MM and EO interface has resulted in uniform sliding or de-bonding of cellulosic fiber from the MM matrix [Soboyejo, 2003]. This uniform narrower de-bonding suggests that more work was performed to fracture the M5E5 specimen. Therefore, surface roughness illustration in Figure 3.21 helps to explain the high value of 28-day fracture toughness of M5E5 sample compared to M7E3 and M6E4 samples [Zum Gahr, 1998; Pukanszky and Voros, 1993; Qiao, 2003; Zhu *et al.,* 1999].

Figure 3.20: The fractured M5E5 specimen and the crack surfaces with protruding cellulosic fibers

The above discussion supports the fact that composites with same volume fraction constituents exhibit higher fracture toughness compared to MM-EO composites containing lesser EO content [Du *et al*., 2006]. This would also mean that inter-facial shearing between MM and cellulosic fiber in EO are pertinent and supports the 28 day data of fracture toughness variation enumerated in Figure 3.15 [Chamis, 1972; Haspel *et al*., 2015; Sockalingam and Nilakantan, 2012; Zhandarov and Mader, 2005; Zhandarov *et al*., 2001]. It is difficult to model the fracture toughness of these particulate composite [German, 2016]. The difficulty may be due to heterogeneous makeup and feeble MM-EO interface [German, 2016].

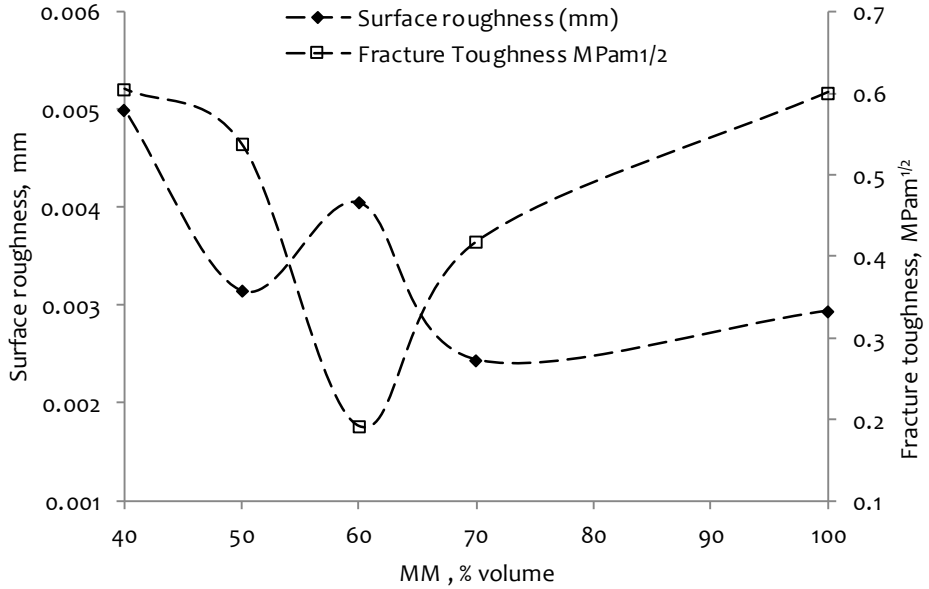

Figure 3.21: The roughness values of M5E5 specimen surfaces compared with surface roughness of other specimens.

3.4 SUMMARY AND CONCLUDING REMARKS

The sustainable use of equal volume fractions of MM and EO in construction of cantilever shelves in rural households is justified and supported. The major finding in this empirical study and its statistical analysis is elaborated in the following lines.

The thermal conductivity of pure MM mirrors again in the composite with 50% volume fraction of EO and MM. A novel multi-parameter model for thermal conductivity of MM-EO composites as a function of mass is proposed.

Density development in composites with distinct constituent volume fractions followed a birth-death process as a function of age. A new stochastic multi-parameter model of density variation as a function of time and distinct composition constant is proposed.

The cellulose fiber $CaCO_3$ content within EO makes it an important commodity in construction materials as well as paper manufacturing industry. Composite samples with approximately 50% by volume of EO showed negligible weight loss with time after a week curing. This stability in weight encourages densification due to dilation or feature of shrinkage.

Resistance to flexural forces increases with increase in age for different composite with distinct compositions. A new quotient response multi-parameter model for flexural strength as a function of time [Plappally *et al.,* 2011]. M5E5 attains the maximum flexural strength compared to composite with other distinct compositions.

Shearing or sliding of cellulosic fiber is observed in fracture experiments. Roughness of the surface is observed to describe the toughness properties of these composites. Roughness of surface may be a new predictor to model toughness of such fiber reinforced composites.

It is important to note the transient nature properties of toughness of the MM-EO composite. Indoor MM-EO composite cantilever shelves within different rural residential buildings are more than two decades old. They have a decadal maintenance cycle which may mean that they require two services during a span of 20 years. This may point towards a requirement of long-term property characterization rather than a 28-days study cycle.

…